

Quantifying the transverse deformability of double-walled carbon and boron nitride nanotubes using an ultrathin nanomembrane covering scheme

Meng Zheng, Lian-feng Zou, Howard Wang, Cheol Park, and Changhong Ke

Citation: *J. Appl. Phys.* **112**, 104318 (2012); doi: 10.1063/1.4766758

View online: <http://dx.doi.org/10.1063/1.4766758>

View Table of Contents: <http://jap.aip.org/resource/1/JAPIAU/v112/i10>

Published by the [American Institute of Physics](#).

Related Articles

Mechanically robust Si nanorod arrays on Cu/Ti bilayer film coated Si substrate for high performance lithium-ion battery anodes

J. Appl. Phys. **112**, 103502 (2012)

Temperature dependent elastic constants and ultimate strength of graphene and graphyne

J. Chem. Phys. **137**, 194901 (2012)

Free volume change of elongated polyethylene films studied using a positron probe microanalyzer

Appl. Phys. Lett. **101**, 203108 (2012)

Molecular dynamics study of dynamical contact between a nanoscale tip and substrate for atomic force microscopy experiments

J. Appl. Phys. **112**, 094325 (2012)

Compression studies of face-to-face π -stacking interaction in sodium squarate salts: $\text{Na}_2\text{C}_4\text{O}_4$ and $\text{Na}_2\text{C}_4\text{O}_4 \cdot 3\text{H}_2\text{O}$

J. Chem. Phys. **137**, 184905 (2012)

Additional information on *J. Appl. Phys.*


Journal Homepage: <http://jap.aip.org/>

Journal Information: http://jap.aip.org/about/about_the_journal

Top downloads: http://jap.aip.org/features/most_downloaded

Information for Authors: <http://jap.aip.org/authors>

ADVERTISEMENT



Special Topic Section:
PHYSICS OF CANCER

Why cancer? Why physics? [View Articles Now](#)

Quantifying the transverse deformability of double-walled carbon and boron nitride nanotubes using an ultrathin nanomembrane covering scheme

Meng Zheng,¹ Lian-feng Zou,¹ Howard Wang,¹ Cheol Park,^{2,3} and Changhong Ke^{1,a)}

¹*Department of Mechanical Engineering, State University of New York at Binghamton, Binghamton, New York 13902, USA*

²*National Institute of Aerospace, 100 Exploration Way, Hampton, Virginia 23666, USA*

³*Department of Mechanical and Aerospace Engineering, University of Virginia, Charlottesville, Virginia 22904, USA*

(Received 27 June 2012; accepted 24 October 2012; published online 20 November 2012)

We investigate the characterization of the transverse deformability of double-walled carbon and boron-nitride nanotubes (i.e., DWCNTs and DWBNNTs) using an ultrathin nanomembrane covering scheme. Monolayer graphene oxide sheets (MGOSs) with a sub-nm thickness are used to cover individual double-walled nanotubes on flat substrates. Nanotube cross-section height reduction occurs due to the compression force exerted by the covering membrane, whose morphological conformation is governed by its bending/stretching rigidities and adhesion interaction with the substrate, as well as the radial height and rigidity of the underlying nanotube. The actual transverse deformation of the underlying tube and its effective radial modulus are quantified through interpreting the measured structural morphology of the covering membrane and the nanotube cross-section height reduction using nonlinear structural mechanics and Hertzian contact mechanics theories. The radial deformations in MGOS-covered tubes are found to positively correlate with the nanotube radial rigidity, thus, increasing with the nanotube outer diameter and decreasing with an increase of the number of tube walls. Our results reveal prominent radial strains of about 20% for DWCNTs of 3.55 nm in outer diameter, while about 24% for DWBNNTs of 3.85 nm in outer diameter. Our data about the effective radial moduli of individual DWCNTs and DWBNNTs are in reasonably good agreement with those obtained using atomic force microscopy-based compression methods. Our work shows that the nanomembrane covering scheme is promising as a quantitative technique for studying the radial rigidity of individual tubular nanostructures. © 2012 American Institute of Physics. [<http://dx.doi.org/10.1063/1.4766758>]

I. INTRODUCTION

Carbon and boron nitride nanotubes (i.e., CNTs and BNNTs) are two types of one-dimensional tubular nanostructures with similar atomic architectures.^{1–3} CNTs are made of covalent C-C bonds, while BNNTs are composed of partially ionic B-N bonding networks. Both CNTs and BNNTs possess extraordinary and largely comparable mechanical, thermal, and chemical properties.⁴ However, their electrical properties are distinctly different. Unlike the metallic or semiconductive properties for CNTs, BNNTs are excellent insulators with band gaps of about 5–6 eV.^{2,5,6} Radial deformability of both types of tubes is important to their structural and physical properties. The radial rigidities of these tubular nanostructures determine whether they undertake circular or hexagonal cross-sectional configurations in tube bundles⁷ or flattened configurations when they are in contact with other materials surfaces.⁸ Both experimental and theoretical studies show that the radial deformations of CNTs and BNNTs have influential impacts on their electronic structures (e.g., band gaps) and conductivities.^{9–15} Therefore, understanding the radial deformability of these tubular nanostructures and ultimately having a good command

of their radial deformations are of great significance to the tuning of their structural, mechanical, and electrical properties and applications.

The most commonly used method to characterize the radial deformability of nanotubes is the atomic force microscopy (AFM)-based compression testing technique,^{15–22} in which a sharp AFM tip is controlled to transversely compress individual tubes lying on flat substrates. Nanotubes deform elastically under relatively small compressive loads and their effective radial moduli, a key physical quantity representing their radial deformability, can be quantified by interpreting the measured nanotube cross-section height versus compressive load profiles using contact mechanics theories. Under large compressive loads, nanotubes undertake substantial transverse deformations and may eventually deform plastically.²² Therefore, substantial permanent radial deformations in individual nanotubes can be manufactured with high spatial resolutions using this AFM nanomanipulation technique, which has been experimentally demonstrated.^{22,23} It is noted that the AFM-based nanotube radial deformation engineering approach is a sequential and slow process as it typically requires multiple visualization and manipulation steps. Therefore, it is practically infeasible for large scale manipulation and integration. Recently, a new ultrathin nanomembrane covering scheme capable of manufacturing prominent radial deformations in CNTs and

^{a)}Author to whom correspondence should be addressed. Email: cke@binghamton.edu. Telephone: 1-607-777-4782. Fax: 1-607-777-4620.

BNNTs in a simple and scalable manner was proposed and demonstrated by our research group.²⁴ By covering individual nanotubes using monolayer graphene oxide sheets (MGOSs), substantial radial deformations occur to the covered tube segment, which is ascribed to the fact that the covering MGOS conforms to and transversely compresses the underlying tube as a result of its adhesion binding interaction with the substrate. For single-walled CNTs and BNNTs (i.e., SWCNTs and SWBNNTs), our prior studies reveal that the magnitude of the engineered nanotube radial deformation using the MGOS covering scheme is inversely correlated to the nanotube outer diameter. Because the effective radial moduli of tubular nanostructures depend on their geometric configurations (e.g., the number of tube walls and the outer diameter), it is plausible that the radial deformability of nanotubes can be quantified using this membrane covering scheme through correlating their effective radial moduli with their geometric configurations and membrane covering-induced radial deformations. Technically, the membrane covering scheme allows the quantification of the radial deformability of the underlying nanotube through measuring its cross-section heights for both the uncovered and the membrane-covered tube segments, which can be handily carried out inside an AFM with a sub-angstrom vertical displacement detection resolution.

In this paper, we investigate the quantification of the radial deformability of double-walled CNTs and BNNTs (i.e., DWCNTs and DWBNNTs) using the membrane covering scheme. We choose double-walled nanotubes (DWNTs) made of carbon and boron-nitride as our model systems in this study for several reasons. First, these DWNTs are structurally the simplest multi-walled nanotubes and have recently attracted a great deal of attention due to their superior mechanical and electrical properties as well as the unique freedom for surface modification of their outer walls while keeping their inner walls intact.²⁵ They are being pursued for a variety of engineering applications, such as nanocomposites,^{26,27} electronics,^{28–30} transport,³¹ and sensing devices.³² Second, determining the number of tube walls in individual nanotubes is an essential, but challenging task in our study, because the commonly used high resolution transmission electron microscopy (HRTEM) technique can not be utilized to visualize nanotubes staying on Si substrates. We employ a nanotube flattening technique^{19,21} to quantify the number of tube walls in each nanotube by means of measuring its cross-section height when it is transversely compressed to nearly flattened configurations. Theoretically, the cross-section height of a completely flattened tube shall be proportional to its number of tube walls. Using tubes of few wall numbers simplifies this task and helps to reduce the error in assigning the number of tube walls. Third, since the radial rigidity of nanotubes increases with their numbers of walls, the radial deformation induced by the membrane covering may become minuscule and undetectable for tubes with a large number of tube walls. Last, the knowledge of the radial deformability of DWNTs obtained in our study is useful to a better understanding of the load transfer and energy absorption mechanisms in these transversely compressed tubular nanostructures and to the development of

theoretical tools capable of predicting their transverse mechanical properties and optimizing design and performance of their structural and mechanical applications (e.g., nanocomposites). By using high resolution AFM imaging techniques, the engineered radial deformations in both DWCNTs and DWBNNTs as a result of MGOS-covering are found to expectedly increase with their outer diameters and be substantially smaller than those of their respective single-walled counterparts with the same outer diameter. The effective radial modulus of each tested tube is quantified based on its measured radial height reduction using a contact mechanics model and is found to be consistent with those obtained using the AFM-based compression method. Our results show that the membrane covering scheme is not only useful to manipulate radial deformations in individual nanotubes in a simple and scalable fashion but also promising as a quantitative technique for studying the radial rigidity of individual nanotubes.

II. RESULTS AND DISCUSSION

A. The membrane-covering-nanotube scheme and governing equations

The membrane-covering-nanotube scheme is illustrated in Figure 1(a), in which one DWNT lying on a flat substrate is partially covered by a thin and uniform membrane.²⁴ Figure 1(b) shows schematically the cross-sections of a DWNT with a height of h_0 (left) and the corresponding membrane-covered tube configuration with a reduced height h and a membrane spanning width L (right), respectively. The reduced nanotube cross-section height h refers to the height difference of the membrane from the position right on top of the underlying tube to its position of the flat covering of the substrate. The membrane conforms to the underlying tube as a result of a balanced competition between the membrane's bending and stretching stiffnesses and the adhesion interactions of the membrane with the substrate and the nanotube. Consequently, the membrane imposes a compressive load P to mechanically deform the underlying tube along its transverse direction. The existence of the underlying tube essentially enforces the delamination of the membrane from the substrate. The separation of the two delamination fronts at $x = \pm L/2$ defines the spanning width (L) of the covering membrane. Therefore, the structural morphology of the covering membrane is governed by its bending and stretching rigidities and adhesion interaction with the substrate as well as the radial height and rigidity of the underlying tube. Figure 1(c) illustrates the free-body diagram for one-half of the covering membrane including the adhesion interactions of the membrane with the nanotube and the substrate. The membrane is subjected to a vertical shear force V_B (per unit length, same for all other forces), a horizontal normal force T_B , and a bending moment M_B at the position B . f_{sm} and f_{tm} represent the vertical forces exerted on the membrane (m) by the substrate (s) and the tube (t), respectively. It is noted that the normal force T_B is balanced by the shear and friction forces between the membrane and the substrate/the nanotube, which are not shown in Figure 1(c) and are strong enough to keep the membrane at a standstill. In the absence

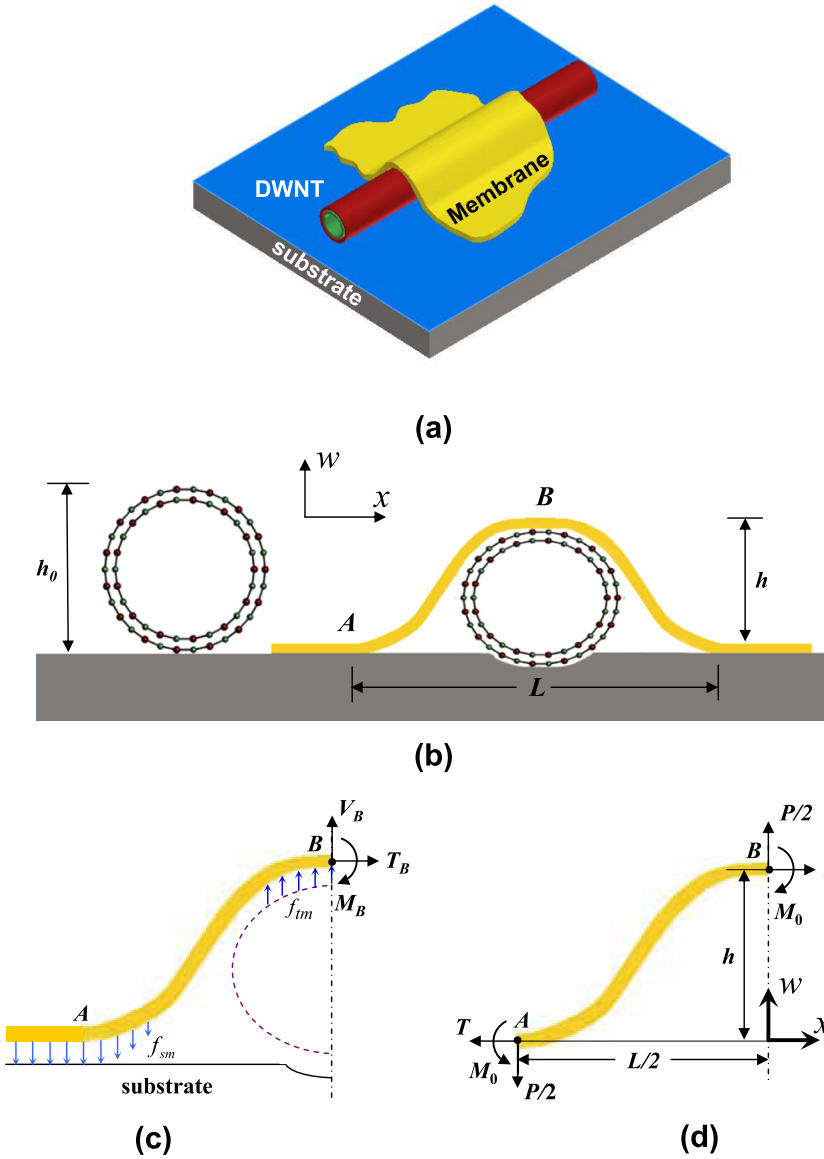


FIG. 1. (a) Schematic of a DWNT on a flat substrate partially covered by a thin membrane. (b) Schematics of the cross-sections of a DWNT (left) and a membrane-covered DWNT (right) on a flat substrate. (c) Free-body diagram of one-half of the covering membrane with the consideration of the adhesion interactions of the membrane with the nanotube and the substrate. The dotted curve represents one-half of the tube cross-section. (d) Simplified free-body diagram of the covering membrane segment AB with the lumped loads at its ends.

of humidity, all these adhesion interaction forces can be ascribed as the van der Waals (vdW) interactions and be modeled using the Lennard-Jones potential, provided that the exact atomic composition and configuration of the contacting bodies are known. It is noted that the substrate-regulated nanomembrane deformations have recently been studied based on a monolayer graphene model using both continuum and molecular mechanics theories.^{33–35} For nanomembranes such as MGOSs used in this study, the exact atomic composition and configuration of the contacting interface are typically unknown. Therefore, it is prudent to employ a simplified atomic or continuum model. In this study, we adopt a continuum mechanics model and take into account the adhesion interaction forces using lumped forces and moments, which are illustrated in the simplified free body diagram shown in Figure 1(d). At the position B, the membrane is subjected to a vertical force $P/2$, one-half of the compressive load applied on the nanotube, a stretching force T and a bending moment M_0 . As a result of equilibrium, the same set of loads of opposite directions is applied on the

membrane at the delamination front A. The structural morphology of the covering membrane, $w(x)$, is given by²⁴

$$D_m \frac{d^2 w}{dx^2} = T \times w + M_0 - \frac{P}{2} \left(\frac{L}{2} + x \right), \quad (1)$$

where $D_m = \frac{E_m t^3}{12(1-\nu_m^2)}$ is the bending stiffness of the membrane with E_m , t , and ν_m as its Young's modulus, thickness, and Poisson's ratio, respectively. The stretching force in the membrane T can be estimated from the length increase of the membrane as revealed by our prior study²⁴ and is given by

$$T = E_m t \frac{\Delta L}{L} = \frac{2E_m t}{L} \left(\int_{-L/2}^0 \sqrt{1 + \left(\frac{dw}{dx} \right)^2} dx - \frac{L}{2} \right). \quad (2)$$

It is noted that L , the spanning width of the covering membrane, is a physical quantity that is measured directly from the experiment. The bending moment at the delamination front M_0 can be obtained from its balanced equilibrium with

the adhesion interaction of the membrane with the substrate and is given by^{36–38}

$$M_0 = \sqrt{2G \times D_m}, \quad (3)$$

where G is the adhesion energy per unit area or energy release rate at the delamination front. The corresponding boundary conditions for the deformed membrane shown in Figure 1(d) are given as follows:

$$\begin{aligned} &\text{At the delamination fronts } (x = \pm L/2), \\ &w = 0 \text{ and } dw/dx = 0; \end{aligned} \quad (4a)$$

$$\text{At the middle point } (x = 0), w = h, \text{ and } dw/dx = 0. \quad (4b)$$

For a given compressive load P , the structural morphology of the covering membrane can be obtained by numerically solving the equation sets (1) to (3) together with the boundary conditions in Eqs. (4a) and (4b). In addition to the numerical solution, a closed-form analytical solution is desired to understand the correlation among all the relevant physical quantities in a simple and straightforward manner.

The boundary conditions given in Eq. (4) suggest that the morphology of the covering membrane can be approximated by the following third-order polynomial equation:

$$w(x) = 4h \left(3 \left(\frac{x}{L} + \frac{1}{2} \right)^2 - 4 \left(\frac{x}{L} + \frac{1}{2} \right)^3 \right), \quad x = [-L/2, 0]. \quad (5)$$

By inserting Eq. (5) into Eq. (1) and applying the boundary conditions, we can obtain

$$P = (4hT + 8M_0)/L. \quad (6)$$

For the covering membrane with a small slope that was revealed by our AFM measurements (i.e., $\frac{dw}{dx} \ll 1$), the stretching force T in the membrane can be approximated as $T = \frac{12tE_m h^2}{5L^2}$ by applying Eq. (5) into Eq. (2) and considering that $\sqrt{1 + \left(\frac{dw}{dx}\right)^2} \approx 1 + \frac{1}{2} \left(\frac{dw}{dx}\right)^2$. Therefore, the compressive load P can be obtained from Eq. (6) as

$$P = \frac{48E_m t h^3}{5L^3} + \frac{8}{L} \sqrt{\frac{G}{6} \frac{E_m t^3}{1 - \nu_m^2}}. \quad (7)$$

It can be clearly seen from Eq. (7) that the compressive load P is positively correlated with the quantities E_m , t , h , and G , while inversely correlated with the membrane spanning width L . It is shown in Sec. II B that the results obtained from Eq. (7) agree well with those numerical solutions obtained directly from solving Eq. (1).

From the measured nanotube height reduction and the calculated compressive load P , the effective radial modulus of the underlying tube is quantified using a contact mechanics model. For thin membranes with high Young's modulus (e.g., graphene and MGOS), their deformations along the thickness direction can be reasonably ignored. Therefore, the

nanotube height reduction, $\Delta h = h_0 - h$, is ascribed to the deformations of the nanotube and the substrate. The nanotube-substrate contact system is simplified as a cylindrical body in contact with a flat substrate under a uniformly distributed compressive line load P . Here, the effect of vdW interactions between the tube and the substrate on the flattening of the tube cross-section⁸ is neglected and the original uncovered nanotube is assumed to undertake a perfectly circular cross-section. The combined nanotube-substrate deformation equals the nanotube cross-section height reduction $\Delta h = h_0 - h$ and is given by³⁹

$$\Delta h = P \left(\frac{1 - \nu_{nt}^2}{\pi E_{nt}} + \frac{1 - \nu_{sub}^2}{\pi E_{sub}} \right) \left[1 + \log \left(\frac{2a^2}{Ph_0 \left(\frac{1 - \nu_{nt}^2}{\pi E_{nt}} + \frac{1 - \nu_{sub}^2}{\pi E_{sub}} \right)} \right) \right], \quad (8)$$

where E_{nt} is the effective radial modulus of the nanotube and E_{sub} is the Young's modulus of the substrate. ν_{nt} and ν_{sub} are the Poisson's ratios of the nanotube and the substrate, respectively. a is the length of the nanotube segment covered by the membrane. The effective radial modulus of the nanotube E_{nt} can be obtained numerically from Eq. (8), provided that the compressive load P and the nanotube height reduction Δh are known. Below, we demonstrate that the quantification of the effective radial moduli of DWCNTs and DWBNNTs using the above-mentioned governing equations for the membrane-covering-nanotube scheme.

B. AFM measurements of MGOS-covered nanotubes

The MGOS-covered nanotube samples were prepared by following the protocol reported in our prior study,²⁴ which is briefly described here. The employed DWCNTs and DWBNNTs were synthesized using chemical vapor deposition (CVD)⁴⁰ and pressurized vapor/condenser (PVC) methods,⁴¹ respectively. GO sheets were synthesized following a previously reported method,⁴² with a carbon to oxygen atomic ratio of 2.06 measured using X-ray photoelectron spectroscopy (XPS). Both CNTs and BNNTs were dispersed in an aqueous solution using ultrasonication with the aid of ionic surfactants.²¹ Dispersed nanotubes were first deposited on clean Si wafers and subsequently rinsed multiple times with deionized (DI) water to remove residue surfactants, followed by the deposition of the GO sheet suspension in DI water by means of spin coating. All the GO sheet-covered nanotube samples were dried at 90 °C for 12 h. The HRTEM images shown in Figures 2(a) and 2(b) display the representative DWCNT and DWBNNT samples employed in our study.

The GO-covered nanotube samples were examined using a Park Systems XE-70 AFM operating at room temperature inside a sealed chamber backfilled with dry nitrogen gas. The employed AFM operates in contact mode using silicon AFM probes (model CSG 01, NT-MDT) with nominal spring constants of 0.01–0.08 N/m. The actual spring constant of each employed AFM cantilever was calibrated using the thermal tuning method based on equipartition theory^{43,44} and was found to be in the range of 0.04–0.09 N/m. The thermal-induced rms deflection noise of the employed AFM

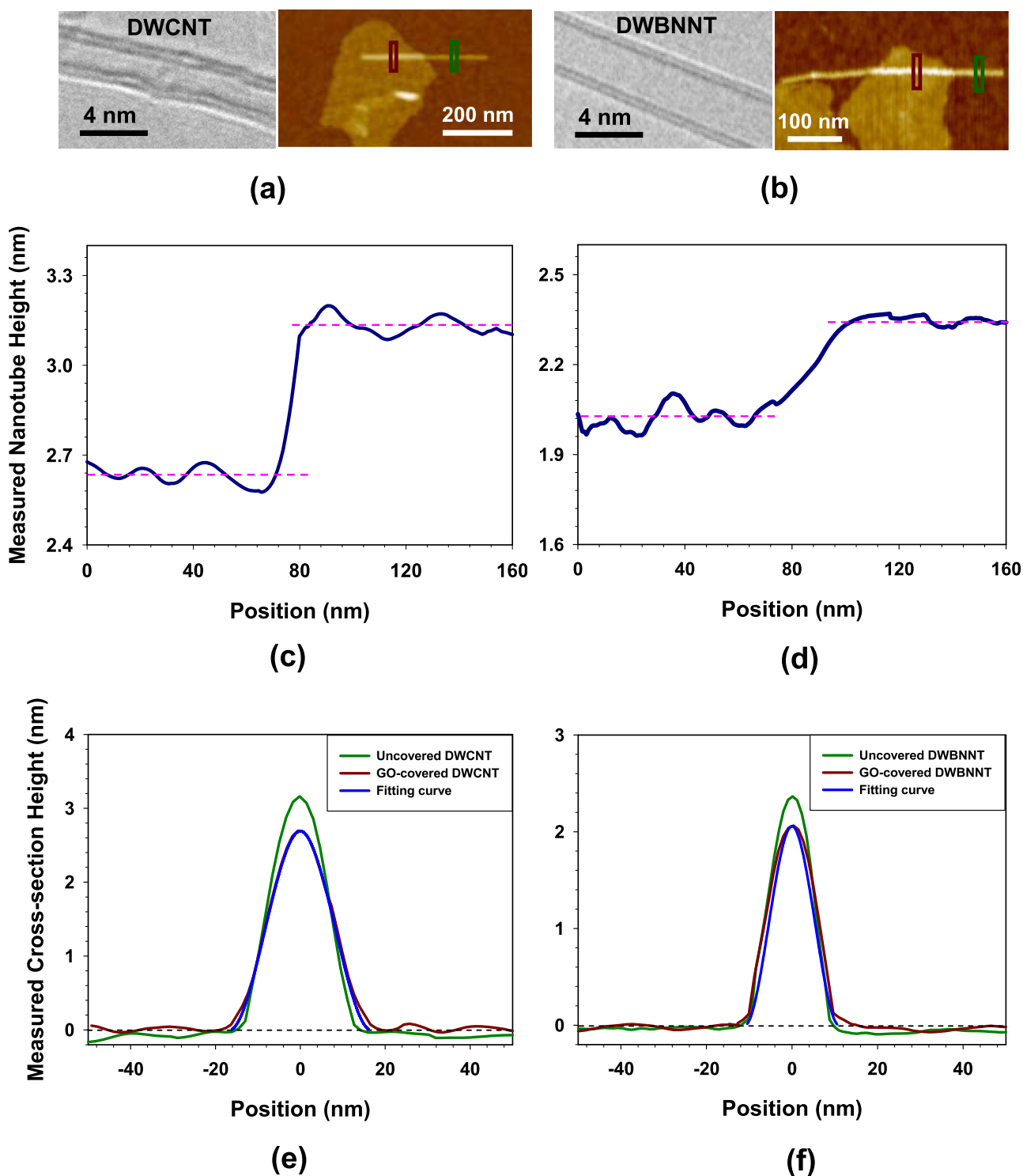


FIG. 2. (a) Representative HRTEM image of one DWCNT (*left*) and AFM image of one MGOS-covered DWCNT (*right*). (b) Representative HRTEM image of one DWBNNT (*left*) and AFM image of one MGOS-covered DWBNNT (*right*). (c) and (d) The measured tube height in the vicinity of the covering membrane edge for the MGOS-covered tubes shown in (a) and (b), respectively. The horizontal axis represents the position along the nanotube axis. (e) and (f) Comparison of the respective cross-section profiles of the uncovered portion (dark green curve) and the MGOS-covered portion (dark red curve) of the tubes shown in (a) and (b), respectively. The profiles are plotted based on the measured height data marked in the green and red boxes shown in the AFM images in (a) and (b). The blue-color fitting curves are plotted based on Eq. (5) for the respective profiles in dark red.

probes at the tip position in the 1-500 Hz bandwidth was measured to be 0.71 \AA using the laser reflection scheme, and the corresponding rms force noise is calculated to be about 3-7 pN. For AFM imaging measurements, a set point of 0.05 nN was used to minimize its impact on the structural mor-

phologies of both the covering membrane and the underlying nanotube. Our AFM imaging measurements show that MGOS has a height of 1.5 nm with a rms value of 0.1 nm on flat Si substrates. Only MGOS-covered nanotubes were selected for analysis.

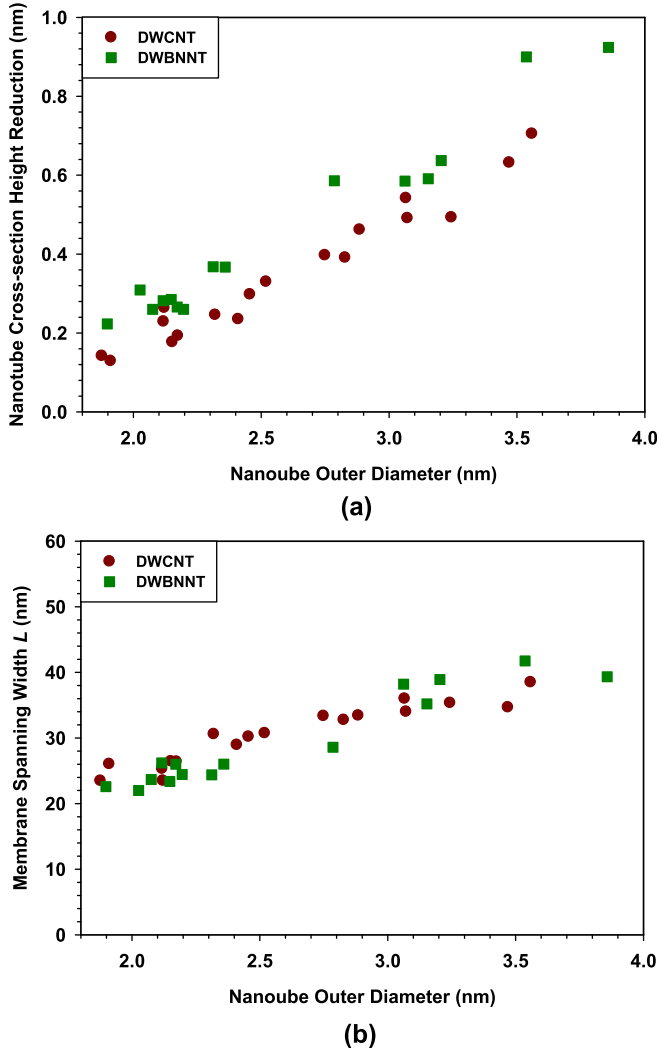


FIG. 3. (a) The respective dependences of the measured cross-section height reduction for MGOS-covered DWCNTs and DWBNNTs on the nanotube outer diameter. (b) Experimentally measured MGOS spanning length L .

The AFM image in Figure 2(a) shows one MGOS-covered CNT, in which the left portion of the tube is covered by the membrane. Figure 2(c) shows the variation of the nanotube height around the edge of the covering membrane, which displays a sharp transition at the position of the membrane edge. The uncovered tube cross-section height is measured to be about 3.15 nm, while about 2.62 nm for the height of the covered tube segment, both of which are marked by the dotted lines in Figure 2(c). Therefore, the cross-section

height reduction for this tube as a result of the MGOS covering is $\Delta h = 0.53$ nm. The green and red curves in Figure 2(e) show the respective cross-section profiles of the uncovered and the MGOS-covered portions of the nanotube based on the AFM-measured height data marked in the green and red boxes in Figure 2(a). The membrane spanning width L for this tube is measured to be 34 nm from the red curve. Similar measurements on one MGOS-covered BNNT are shown in Figure 2(b). From the measured curves presented in Figures 2(d) and 2(f), the original and the MGOS-covered tube heights are measured to be 2.37 nm and 2.06 nm, respectively, indicating a height reduction of 0.31 nm. The corresponding membrane spanning width L is measured to be 22 nm. Figures 2(e) and 2(f) also include the respective fitting curves (blue curves with R-squared values of 99.9% and 99.1%, respectively) to the AFM measured GO-covered nanotube profiles (red curves) based on Eq. (5), which display good agreement. Our results clearly show that the structural morphology of the covering membrane can be reasonably approximated by Eq. (5).

Figure 3(a) shows the dependences of the nanotube cross-section height reduction as a result of the MGOS covering on the nanotube outer diameter, based on measurements of 18 different BNNTs and 15 different CNTs, whose original tube outer diameters are measured to be within 1.9 to 3.9 nm. The nanotube outer diameter here is defined as $D_{nt} = h_0 - t_{nt}$, in which $t_{nt} = 0.34$ nm is the inter-layer distance of both the graphene and B-N sheets.^{19,41} One of the essential tasks is to ensure that the tubes we analyzed are indeed double-walled. We performed nanotube flattening measurements²¹ on some of the tested BNNTs and CNTs to determine their numbers of tube walls and the key measured and calculated data are listed in Table I for six selected tubes. For nanotube flattening tests, the extruding portion of a MGOS-covered nanotube is squeezed by the same AFM tip used for imaging with a compressive load of 50 nN. To minimize the effect of the covering membrane, the position chosen for the flattening test is away from the edge of the covering membrane. It is noted that both the AFM tip and the substrate deform as well during the nanotube flattening process. Therefore, the actual cross-section height of a nearly flattened nanotube is calculated as the measured tube cross-section height plus the combined deformation of the AFM tip and the substrate, the latter of which is estimated using a Hertzian contact model. The contacts among the AFM tip, the nanotube and the substrate are simplified as a

TABLE I. List of the key experimentally measured and calculated parameters in the nanotube flattening measurements for six selected MGOS-covered CNT and BNNT samples.

Sample #	Original tube cross-section height (nm)	Measured tube height at $P = 50$ nN (nm)	Combined AFM tip and substrate deformation at $P = 50$ nN (nm)	Actual tube height at $P = 50$ nN (nm)	Assigned number of tube walls
CNT #1	2.80	0.94	0.56	1.50	2
CNT #2	2.46	0.98	0.60	1.58	2
CNT #3	3.23	0.95	0.52	1.47	2
BNNT #1	3.20	0.94	0.50	1.44	2
BNNT #2	2.79	0.92	0.53	1.45	2
BNNT #3	2.15	0.95	0.59	1.54	2

nanindentation system including a spherical tip, a cylindrical tube and a flat substrate. By assuming the tube is a rigid body, the combined deformation of the AFM tip and the substrate Δ is estimated as^{16,22}

$$\Delta = \left[\frac{3}{4} \left(\frac{1 - \nu_{sub}^2}{E_{sub}} \right) \frac{P}{\sqrt{h_0}} \right]^{2/3} + \left[\frac{3}{4} \left(\frac{1 - \nu_{tip}^2}{E_{tip}} \right) \frac{P}{\sqrt{[1/h_0 + 1/R_{tip}]^{-1}}} \right]^{2/3}, \quad (9)$$

where E and ν represent the elastic modulus and the Poisson's ratio, respectively, for materials of the AFM tip (subscript-*tip*) and the substrate (*sub*). The first term on the right side of Eq. (9) represents the deformation of the substrate, while the second term represents the deformation of the AFM tip. The materials for both the AFM tip and the substrate are considered to be native silicon oxide with an elastic modulus of 74 GPa and a Poisson's ratio of 0.16.²² The radius of curvature of the employed AFM tips, R_{tip} , is estimated to be about 25 nm based on the geometrical deconvolution relationship $R_{tip} = \omega^2/8\Delta$, in which Δ and ω are the measured height and the apparent width of a nanotube in the AFM scanning image.⁴⁵ All six tubes listed in Table I are confirmed to be double-walled based on their flattened tube heights, which are found to be in the range of 1.44–1.58 nm, quite close to the theoretical value of 1.36 nm for a completely flattened DWCNT or DWBNNT.

Our data presented in Figure 3(a) consistently show that, for both types of tubes, the nanotube height reduction increases with the nanotube outer diameter, indicating that the nanotube height reduction is positively correlated with its radial rigidity. This observation is also consistent with the fact that DWBNNTs deform more in their transverse direction as a result of the MGOS covering compared with DWCNTs of the same outer diameter, which can be ascribed to the fact that DWBNNTs possess relatively lower effective radial moduli than their pure carbon counterparts.^{21,46} Figure 3(b) shows the measured membrane spanning width for all the tested tube samples. For both CNTs and BNNTs, the measured membrane spanning width displays a comparable and slightly increasing trend with the nanotube outer diameter.

C. Effective radial moduli of DWCNTs and DWBNNTs

The effective radial moduli of those DWCNTs and DWBNNTs covered by MGOSs are obtained using Eq. (8) based on the measured nanotube height reduction as shown in Figure 3(a) and the calculated compressive load P that is exhibited in Figure 4. The solid and empty data points in Figure 4 represent the calculations based on Eqs. (1) and (7), respectively, which display good agreement. The following parameters are employed in the calculation: $E_m = 207$ GPa, $t = 0.7$ nm, $\nu_m = 0.19$, and $G = 0.038$ J/m².²⁴ The average difference between the results for the MGOS-covered BNNTs is 4%, while 2.7% for the MGOS-covered CNTs. Our results show that Eq. (7) can be used confidently to

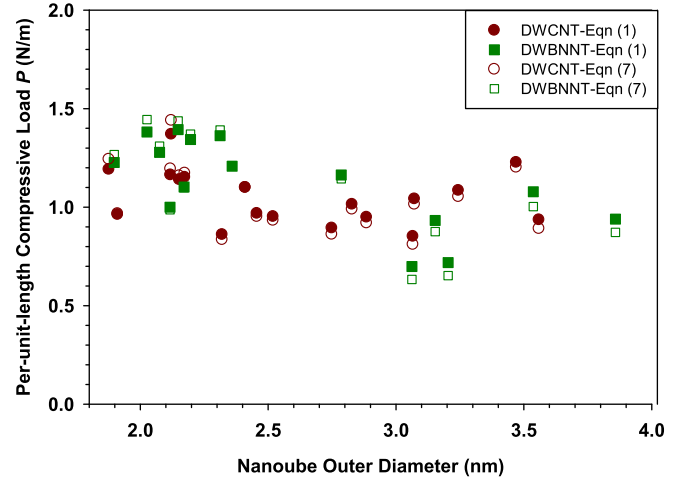


FIG. 4. The dependences of the calculated per-unit-length compressive load applied on DWCNTs and DWBNNTs on the nanotube outer diameter. The solid circles and squares represent results obtained based on Eq. (1), while the empty circles and squares represent results obtained based on Eq. (7).

predict the compressive load applied on the underlying nanotube by the covering membrane. Furthermore, the correlations among all the involved quantities revealed by Eq. (7) are useful for the design and optimization of the membrane covering scheme for the purpose of engineering the radial deformation in tubular nanostructures.

The effective radial moduli of the tested tube samples, calculated using Eq. (8), are shown in Figure 5. Our results show that the effective radial moduli for both types of tubes expectedly decrease with an increase of the tube outer diameter and DWCNTs possess higher effective radial moduli than DWBNNT of the same outer diameter. It is noted that the data corresponding to those tubes characterized in the nanotube flattening tests and listed in Table I follow their respective trends very well and provide a strong support that all the tubes presented in this paper are double-walled. For a comparison purpose, Figure 5 also includes the data about the

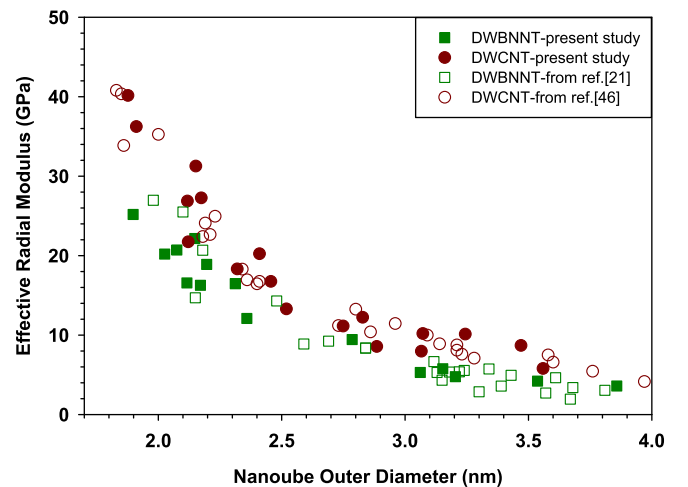


FIG. 5. Comparison between the calculated effective radial modulus data for DWCNTs (solid circles) and DWBNNTs (solid squares) based on Eq. (8) with those data reported in the literature. The DWBNNT data represented by empty squares are reproduced from Ref. 21; while from Ref. 46 for the DWCNT data represented by empty circles.

effective radial moduli of both DWCNTs and DWBNNTs obtained using AFM-based compression methods,^{21,46} which display reasonably good agreements with our data obtained using the MGOS-covering scheme. Our results clearly demonstrate that the membrane covering scheme can be used to quantify the radial rigidity of tubular nanostructures.

We also examine the actual cross-section deformation of the nanotube induced by the MGOS covering. By considering the substrate as a rigid body, the actual radial deformation of the nanotube, δd , can be obtained using Eq. (8). Figure 6 shows the dependences of the actual nanotube radial deformation strain ϵ_{nt}^{rad} , defined as $\epsilon_{nt}^{rad} = \frac{\delta d}{D_{nt}}$, on the tube outer diameter for both DWCNTs and DWBNNTs. Our results show that ϵ_{nt}^{rad} increases, in nearly linear fashion, with the tube outer diameter for both types of tubes. For DWCNTs, the engineered radial strain increases from 7% for tubes of 1.9 nm in outer diameter to 20% for tubes of 3.55 nm in outer diameter. For DWBNNTs, the radial strain increases from 12% to 24% for tube outer diameters in the range of 1.9 to 3.85 nm. Our results reveal that DWBNNTs consistently deform more along their transverse directions than comparable DWCNTs, with the difference of about 3–5% in radial deformation strain within the measured tube diameter range. It is noted that the observed radial deformations for those double-walled tubes are found to be significantly lower than their respective comparable single-walled counterparts, which can be ascribed to their differences in radial rigidity. For a comparison purpose, our recently reported results on the radial deformations of MGOS-covered SWCNTs and SWBNNTs²⁴ are also plotted in Figure 6. For tubes of 2 nm in outer diameter, the MGOS covering induced radial strains in SWCNTs and SWBNNTs are measured to be 29.5% and 40.5%, respectively, compared with 12% for DWCNTs and 16% for DWBNNTs. Therefore, the engineered radial deformation in nanotubes using the membrane-covering scheme decreases with the increase of the number

of tube walls, which is largely expected due to the fact that the nanotube radial rigidity is positively correlated with the number of tube walls.

D. Remarks for future improvement in both experiments and modeling

Our work presented in this paper demonstrates the feasibility of employing the membrane-covering scheme as a quantitative technique to study the radial rigidity of tubular nanostructures. Below, we discuss some of the issues related to both the membrane selection and the modeling of the membrane-covering scheme, which can be considered in the future study of this technique. In our study, MGOS is employed as our model membrane primarily due to its ease in synthesis and processing. Because MGOS is water soluble and can be processed using well-established micro/nanofabrication techniques, the MGOS-covering scheme can be used for large-scale manipulation of radial deformations in nanotubes.²⁴ Besides GO sheets, monolayer or a few layer graphene sheets can be used as the covering membranes due to their high elastic modulus (1 TPa⁴⁸ versus 207 GPa for MGOS⁴⁷) and strong adhesion interaction with the substrate (up to 0.45 J/m² for graphene with Si substrates^{49,50}). Therefore, the compressive load applied on the underlying nanotube from using monolayer graphene is expected to be substantially higher compared with MGOS. It is noted that other factors such as the synthesis, processing, and properties of graphene may also influence its usage in the membrane covering scheme. For instance, graphene is not water-soluble. Therefore, the spin-coating technique used for membrane deposition that works well for MGOS may fail to work for graphene. Graphene is an excellent conductor and will interfere with the electron transport in the underlying nanotube.

The accuracy of the quantification of the nanotube's radial effective modulus relies heavily on the theoretical models about the structural morphologies of the covering membrane and the underlying nanotube. The governing equations presented in this paper are based on simplified continuum models for both the membrane and the nanotube. The adhesion interactions as well as the shear and friction forces among all the contacting bodies are considered in the form of lumped forces. In addition, the deformation of the underlying nanotube involves bending, stretching, and rotation of the chemical bonds in the nanotube. The employed contact mechanics model, on which both Eqs. (8) and (9) are based, is a simplified continuum model that takes into account the deformations of the contacting bodies (i.e., the nanotube and the substrate) based on their simplified geometries and contacting interfaces, while neglecting delicate features such as the effect of the adhesion force on the conformation of the nanotube and the deformation of the bulk Si underneath the oxide layer. For this aspect, our model is valid only for those tubes of relatively small diameters, which possess high radial rigidities and have circular or nearly circular tube cross-sections on flat substrates. More precise modeling of the deformations of the membrane and the nanotube based on advanced computational approaches,

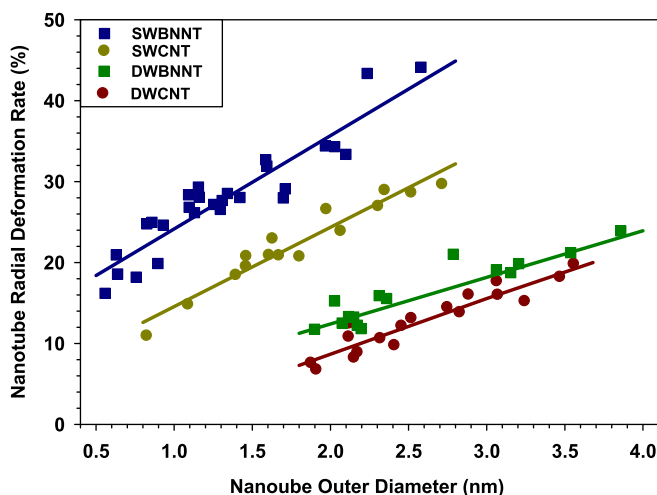


FIG. 6. The respective dependences of the MGOS covering induced actual nanotube radial strain on the nanotube outer diameters for both single- and double-walled CNTs and BNNTs. The data for SWCNTs and SWBNNTs are reproduced from Ref. 24. The solid lines are the linear-fitting curves of the respective data sets.

such as finite element methods (FEM) and molecular dynamics (MD), is warranted in the future study of this technique.

III. CONCLUSIONS

In this paper, we present a study of characterizing the transverse deformability of DWCNTs and DWBNNTs using an ultrathin nanomembrane covering scheme. The structural morphologies of the MGOS-covered nanotube were measured by AFM and interpreted using structural and contact mechanics models. A closed-form analytical solution was derived to predict the compressive load exerted on the underlying tube by the covering membrane. The engineered radial strains in the MGOS-covered tubes are found to increase with the nanotube outer diameter and decrease with the increase of the number of tube walls. Our data on the effective radial moduli of individual DWCNTs and DWBNNTs obtained using the membrane-covering scheme are in reasonably good agreement with those obtained using AFM-based compression methods. Our work shows that the nanomembrane-covering scheme is promising as a quantitative technique for studying the radial rigidity of individual nanotubes.

ACKNOWLEDGMENTS

This work was funded by U.S. Air Force Office of Scientific Research - Low Density Materials Program under Grant Nos. FA9550-11-1-0042 and FA9550-10-1-0451. We thank Dr. In-Tae Bae for his assistance with the TEM characterization. The HRTEM measurements were performed using the facilities in the Analytical and Diagnostics Laboratory at Binghamton University's Small Scale Systems Integration and Packaging Center (S³IP).

¹S. Iijima, "Helical microtubules of graphitic carbon," *Nature* **354**, 56–58 (1991).
²A. Rubio, J. L. Corkill, and M. L. Cohen, "Theory of graphitic boron-nitride nanotubes," *Phys. Rev. B* **49**, 5081–5084 (1994).
³N. G. Chopra, R. J. Luyken, K. Cherrey, V. H. Crespi, M. L. Cohen, S. G. Louie, and A. Zettl, "Boron-nitride nanotubes," *Science* **269**, 966–967 (1995).
⁴D. Golberg, Y. Bando, Y. Huang, T. Terao, M. Mitome, C. C. Tang, and C. Y. Zhi, "Boron nitride nanotubes and nanosheets," *ACS Nano* **4**, 2979–2993 (2010).
⁵X. Blase, A. Rubio, S. G. Louie, and M. L. Cohen, "Stability and band-gap constancy of boron-nitride nanotubes," *Europhys. Lett.* **28**, 335–340 (1994).
⁶C. H. Lee, M. Xie, V. Kayastha, J. S. Wang, and Y. K. Yap, "Patterned growth of boron nitride nanotubes by catalytic chemical vapor deposition," *Chem. Mater.* **22**, 1782–1787 (2010).
⁷M. J. Lopez, A. Rubio, J. A. Alonso, L. C. Qin, and S. Iijima, "Novel polygonized single-wall carbon nanotube bundles," *Phys. Rev. Lett.* **86**, 3056–3059 (2001).
⁸T. Hertel, R. E. Walkup, and P. Avouris, "Deformation of carbon nanotubes by surface van der Waals forces," *Phys. Rev. B* **58**, 13870–13873 (1998).
⁹O. Gulseren, T. Yildirim, S. Ciraci, and C. Kilic, "Reversible band-gap engineering in carbon nanotubes by radial deformation," *Phys. Rev. B* **65**, 155410 (2002).
¹⁰Y. Kinoshita and N. Ohno, "Electronic structures of boron nitride nanotubes subjected to tension, torsion, and flattening: A first-principles DFT study," *Phys. Rev. B* **82**, 085433 (2010).
¹¹V. H. Crespi, M. L. Cohen, and A. Rubio, "In situ band gap engineering of carbon nanotubes," *Phys. Rev. Lett.* **79**, 2093–2096 (1997).

¹²X. D. Bai, D. Golberg, Y. Bando, C. Y. Zhi, C. C. Tang, M. Mitome, and K. Kurashima, "Deformation-driven electrical transport of individual boron nitride nanotubes," *Nano Lett.* **7**, 632–637 (2007).
¹³Y. H. Kim, K. J. Chang, and S. G. Louie, "Electronic structure of radially deformed BN and BC3 nanotubes," *Phys. Rev. B* **63**, 205408 (2001).
¹⁴B. Shan, G. W. Lakatos, S. Peng, and K. J. Cho, "First-principles study of band-gap change in deformed nanotubes," *Appl. Phys. Lett.* **87**, 173109 (2005).
¹⁵A. P. M. Barboza, H. Chacham, and B. R. A. Neves, "Universal response of single-wall carbon nanotubes to radial compression," *Phys. Rev. Lett.* **102**, 025501 (2009).
¹⁶Y. H. Yang and W. Z. Li, "Radial elasticity of single-walled carbon nanotube measured by atomic force microscopy," *Appl. Phys. Lett.* **98**, 041901 (2011).
¹⁷I. Palaci, S. Fedrigo, H. Brune, C. Klinke, M. Chen, and E. Riedo, "Radial elasticity of multiwalled carbon nanotubes," *Phys. Rev. Lett.* **94**, 175502 (2005).
¹⁸M. F. Yu, T. Kowalewski, and R. S. Ruoff, "Investigation of the radial deformability of individual carbon nanotubes under controlled indentation force," *Phys. Rev. Lett.* **85**, 1456–1459 (2000).
¹⁹T. DeBorde, J. C. Joiner, M. R. Leyden, and E. D. Minot, "Identifying individual single-walled and double-walled carbon nanotubes by atomic force microscopy," *Nano Lett.* **8**, 3568–3571 (2008).
²⁰W. D. Shen, B. Jiang, B. S. Han, and S. S. Xie, "Investigation of the radial compression of carbon nanotubes with a scanning probe microscope," *Phys. Rev. Lett.* **84**, 3634–3637 (2000).
²¹M. Zheng, C. H. Ke, I. T. Bae, C. Park, M. W. Smith, and K. Jordan, "Radial elasticity of multi-walled boron nitride nanotubes," *Nanotechnology* **23**, 095703 (2012).
²²M. Zheng, X. M. Chen, I. T. Bae, C. H. Ke, C. Park, M. W. Smith, and K. Jordan, "Radial mechanical properties of single-walled boron nitride nanotubes," *Small* **8**, 116–121 (2012).
²³S. J. Tans, A. R. M. Verschueren, and C. Dekker, "Room-temperature transistor based on a single carbon nanotube," *Nature* **393**, 49–52 (1998).
²⁴M. Zheng, L. F. Zou, H. Wang, C. Park, and C. H. Ke, "Engineering radial deformations in single-walled carbon and boron nitride nanotubes using ultrathin nanomembranes," *ACS Nano* **6**, 1814–1822 (2012).
²⁵D. Bouilly, J. Cabana, F. Meunier, M. Desjardins-Carriere, F. Lapointe, P. Gagnon, F. L. Larouche, E. Adam, M. Paillet, and R. Martel, "Wall-selective probing of double-walled carbon nanotubes using covalent functionalization," *ACS Nano* **5**, 4927–4934 (2011).
²⁶C. Guiderdoni, C. Estournes, A. Peigney, A. Weibel, V. Turq, and C. Laurent, "The preparation of double-walled carbon nanotube/Cu composites by spark plasma sintering, and their hardness and friction properties," *Carbon* **49**, 4535–4543 (2011).
²⁷M. Naraghi, T. Filleter, A. Moravsky, M. Locascio, R. O. Loutfy, and H. D. Espinosa, "A multiscale study of high performance double-walled nanotube-polymer fibers," *ACS Nano* **4**, 6463–6476 (2010).
²⁸T. Morimoto, A. Kuno, S. Yajima, K. Ishibashi, K. Tsuchiya, and H. Yajima, "Effective energy gap of the double-walled carbon nanotubes with field effect transistors ambipolar characteristics," *Appl. Phys. Lett.* **100**, 043107 (2012).
²⁹Y. F. Li, R. Hatakeyama, W. Oohara, and T. Kaneko, "Formation of p-n junction in double-walled carbon nanotubes based on heteromaterial encapsulation," *Appl. Phys. Express* **2**, 095005 (2009).
³⁰A. A. Green and M. C. Hersam, "Properties and application of double-walled carbon nanotubes sorted by outer-wall electronic type," *ACS Nano* **5**, 1459–1467 (2011).
³¹A. Popescu and L. M. Woods, "Telescopic hot double wall carbon nanotube for nanolithography," *Appl. Phys. Lett.* **95**, 203507 (2009).
³²X. C. Dong, D. L. Fu, Y. P. Xu, J. Q. Wei, Y. M. Shi, P. Chen, and L. J. Li, "Label-free electronic detection of DNA using simple double-walled carbon nanotube resistors," *J. Phys. Chem. C* **112**, 9891–9895 (2008).
³³Z. Zhang and T. Li, "Graphene morphology regulated by nanowires patterned in parallel on a substrate surface," *J. Appl. Phys.* **107**, 103519 (2010).
³⁴Z. H. Aitken and R. Huang, "Effects of mismatch strain and substrate surface corrugation on morphology of supported monolayer graphene," *J. Appl. Phys.* **107**, 123531 (2010).
³⁵Z. Zhang and T. Li, "A molecular mechanics study of morphologic interaction between graphene and Si nanowires on a SiO₂ substrate," *J. Nanomater.* **2011**, 374018 (2011).
³⁶C. Ke, M. Zheng, G. Zhou, W. Cui, N. Pugno, and R. N. Miles, "Mechanical peeling of free-standing single-walled carbon nanotube bundles," *Small* **6**, 438–445 (2010).

- ³⁷M. Zheng and C. H. Ke, "Elastic deformation of carbon-nanotube nano-rings," *Small* **6**, 1647–1655 (2010).
- ³⁸C. H. Ke, M. Zheng, I. T. Bae, and G. W. Zhou, "Adhesion-driven buckling of single-walled carbon nanotube bundles," *J. Appl. Phys.* **107**, 104305 (2010).
- ³⁹M. J. Puttock and E. G. Thwaite, *Elastic Compression of Spheres and Cylinders at Point and Line Contact* (Commonwealth Scientific and Industrial Research Organization, Melbourne, Australia, 1969).
- ⁴⁰W. Z. Li, S. S. Xie, L. X. Qian, B. H. Chang, B. S. Zou, W. Y. Zhou, R. A. Zhao, and G. Wang, "Large-scale synthesis of aligned carbon nanotubes," *Science* **274**, 1701–1703 (1996).
- ⁴¹M. W. Smith, K. C. Jordan, C. Park, J. W. Kim, P. T. Lillehei, R. Crooks, and J. S. Harrison, "Very long single- and few-walled boron nitride nanotubes via the pressurized vapor/condenser method," *Nanotechnology* **20**, 505604 (2009).
- ⁴²W. S. Hummers, Jr. and R. E. Offeman, "Preparation of graphitic oxide," *J. Am. Chem. Soc.* **80**, 1339 (1958).
- ⁴³C. Ke, M. Humeniuk, H. S-Gracz, and P. E. Marszalek, "Direct measurements of base stacking interactions in DNA by single-molecule atomic-force spectroscopy," *Phys. Rev. Lett.* **99**, 018302 (2007).
- ⁴⁴E. L. Florin, M. Rief, H. Lehmann, M. Ludwig, C. Dornmair, V. T. Moy, and H. E. Gaub, "Sensing specific molecular-interactions with the atomic-force microscope," *Biosens. Bioelectron.* **10**, 895–901 (1995).
- ⁴⁵C. T. Gibson, G. S. Watson, and S. Myhra, "Scanning force microscopy: Calibrative procedures for 'best practice'," *Scanning* **19**, 564–581 (1997).
- ⁴⁶M. Zheng, X. Chen, C. Park, and C. Ke, "Radial deformability of carbon and boron nitride nanotubes," in *Proceedings of the 23rd International Congress on Theoretical and Applied Mechanics (ICTAM)*, Beijing, China, 2012.
- ⁴⁷J. W. Suk, R. D. Piner, J. H. An, and R. S. Ruoff, "Mechanical properties of mono layer graphene oxide," *ACS Nano* **4**, 6557–6564 (2010).
- ⁴⁸C. Lee, X. D. Wei, J. W. Kysar, and J. Hone, "Measurement of the elastic properties and intrinsic strength of monolayer graphene," *Science* **321**, 385–388 (2008).
- ⁴⁹S. P. Koenig, N. G. Boddeti, M. L. Dunn, and J. S. Bunch, "Ultrastrong adhesion of graphene membranes," *Nat. Nanotechnol.* **6**, 543–546 (2011).
- ⁵⁰Z. Zong, C. L. Chen, M. R. Dokmeci, and K. T. Wan, "Direct measurement of graphene adhesion on silicon surface by intercalation of nanoparticles," *J. Appl. Phys.* **107**, 026104 (2010).